Chemical Vapor Deposition

Full Paper

# Volatile Surfactant-Assisted MOCVD: Application to $LaAlO_3$ Thin-Film Growth**

By *Alexander A. Molodyk, Igor E. Korsakov, Mikhail A Novojilov, Igor E. Graboy, Andrey R. Kaul,* and Georg Wahl*

A new approach to the CVD of oxides with kinetically hindered diffusion, called volatile surfactant-assisted (VSA) metal–organic chemical vapor deposition (MOCVD), consisting of film deposition in the presence of a volatile low melting point oxide ($Bi_2O_3$) has been developed. The process was applied to the deposition of $LaAlO_3$ films, and a model of the process was proposed. Epitaxial and textured $LaAlO_3$ films on various substrates were obtained, both by thermal and VSA MOCVD. A marked improvement in crystalline quality and surface morphology was found for the films deposited by VSA MOCVD. $LaAlO_3$ films obtained in the presence of $Bi_2O_3$ did not contain Bi. A significant increase (up to five times) of the deposition rate was observed for $LaAlO_3$ films deposited by VSA MOCVD compared with that for the films grown by thermal MOCVD.

Keywords: MOCVD, Lanthanum aluminate, Diffusion enhancement, Volatile surfactant, Oxide thin films

## 1. Introduction

The growth of thin films from a gas phase by various deposition techniques results in different film morphologies, textures, and crystallinity. Crystal growth theories regard these properties as being dependent on the interplay of condensation rate and diffusion mobility in the growing film. When diffusivity in the growing film is not high enough to accommodate the flow of the substance coming to the substrate from the gas phase, a polycrystalline or amorphous film grows instead of an oriented or epitaxial one (provided that crystallographic requirements to epitaxy are met). The homologous temperature, which is the ratio of deposition temperature $T_d$ to melting temperature $T_m$, can be used as a measure of diffusivity in the growing film. The Tamman rule says that diffusion-activated processes in solids become active at temperatures of about 0.8–0.6 $T_m$. At typical deposition temperatures not exceeding 1000 °C, it is always difficult to obtain films of high crystalline quality for the phases with high melting temperatures. To solve this problem, diffusion mobility in the growing films must be enhanced.

In some physical vapor deposition (PVD) techniques such as pulsed laser deposition, or ion beam or magnetron sputtering, surface mobility in the growing films is increased due to bombardment of the film surface by energetic particles. Several approaches of non-thermal activation, which affect surface mobility and/or process chemistry, have been developed for CVD, namely, plasma-,[1] photo-,[2] ultraviolet-,[3] and laser-activation,[4] etc. In our recent study,[5] we proposed heterovalent doping, creating a high concentration of ion vacancies in the structure of the material being deposited, as a way to enhance diffusion mobility in the growing film. Both PVD and CVD activated processes allow crystalline films to be obtained at relatively low temperatures.

Lanthanum aluminate ($T_m$ = 2100 °C) is an example of a phase with almost no diffusion at conventional deposition temperatures, but it could have a prospective application as a buffer layer for the growth of various perovskite films such as high-temperature superconductors, ferroelectrics, metal-conducting oxides, and colossal magnetoresistance oxides.[6] However, there have been few reports of the successful deposition of $LaAlO_3$ films of high crystalline quality. The only reports in the literature to date have been of epitaxial $LaAlO_3$ films grown by pulsed laser deposition (PLD),[6,7] radio frequency (RF) magnetron sputtering,[8] and sol-gel[9] on perovskite substrates ($SrTiO_3$ and $LaAlO_3$ itself). Attempts to grow $LaAlO_3$ on Si, MgO, $Al_2O_3$, $CeO_2$, and YSZ led to amorphous, or at best polycrystalline, films.[6,7] Recently, Malandrino et. al. succeeded in obtaining highly (111) oriented $LaAlO_3$ films on (001)YSZ substrates by thermal MOCVD at 1050 °C,[10] as well as (001)$LaAlO_3$ films on (001)$SrTiO_3$.[11]

We tried to accelerate the diffusion mobility in the MOCVD of $LaAlO_3$ films by changing the film growth mechanism to one close to vapor–liquid–solid. It was accomplished by film deposition in the presence of volatile low melting point oxide; in our case bismuth oxide $Bi_2O_3$ was selected. This approach to diffusion and crystallization

[*] Prof. A. R. Kaul, Dr. A. A. Molodyk,[+] Dr. I. E. Korsakov, M. A. Novojilov, Dr. I. E. Graboy
Department of Chemistry, Moscow State University
119899, Moscow (Russia)
Prof. G. Wahl
Institut für Oberflachentechnik
TU Braunschweig
Bienroder Weg 53, D-38108 Braunschweig (Germany)
[+] Present address: CSIRO Telecommunications and Industrial Physics, PO Box 218, Lindfield, Sydney, NSW 2070, Australia.

[**] This work was partly supported by projects COPERNICUS ERB-IC15-CT96-0735 and VW I/73 628. Dr. A. A. Molodyk is grateful to Robert Havemann Stiftung for a fellowship.

  0948-1907/00/0306-0133 $ 17.50+.50/0 

enhancement was used for the first time in our previous study on the MOCVD of $BaTiO_3$ films.[12] At the first stage of this work, the experiments on thermally activated MOCVD in the absence of $Bi_2O_3$ were performed in the temperature range 800–1050 °C.

## 2. Results and Discussion

### 2.1. $LaAlO_3$ Films Deposited Without $BiPh_3$: X-ray Diffraction Characterization

$LaAlO_3$ films were deposited on a number of substrates with different structure types: perovskite type (001)$NdGaO_3$, (110)$SrTiO_3$; fluorite type (001)YSZ and fluorite type buffer layers (001)$PrO_x$/(001)YSZ and (001)$CeO_2$/(1$\bar{1}$02)$Al_2O_3$; NaCl type (001)MgO; and on R-sapphire (1$\bar{1}$02)$Al_2O_3$. Deposition parameters used are listed in Table 1.

Table 1. Parameters of the deposition process.

| Parameter | Value |
|---|---|
| Deposition temperature [°C] | 800–1050 |
| Total pressure [mbar] | 20 |
| Total gas flow [L $h^{-1}$] | 20 |
| Partial pressure of $O_2$ [mbar] | 10 |
| Deposition time [min] | 20–30 |
| Solvent consumption [mL $h^{-1}$] | 20 |
| Total precursor concentration [mol $L^{-1}$] | 0.02 |
| Evaporation temperature [°C] | 250 |

All films with composition close to the stoichiometry obtained at 950 °C and higher, on all the substrates used, were crystalline. Thus, we succeeded in depositing crystalline $LaAlO_3$ films not only on perovskite type substrates but also on the substrates of other structural types, the films deposited at 1000 °C being epitaxial or highly oriented, as will be shown below. The crystalline quality of the films decreased dramatically with even slight deviations of the film composition from molar ratio Al/La = 1:1. Off-stoichiometric films were amorphous. At the lower deposition temperature 900 °C, only $LaAlO_3$ films on perovskite type substrates $NdGaO_3$ were found to be crystalline. As-deposited amorphous films crystallized over a 2 h annealing period at 1000 °C, which again indicated low diffusion mobility of lanthanum aluminate under the deposition conditions.

We believe that correct composition of the films and high growth temperature allowed us to deposit, for the first time, oriented $LaAlO_3$ films on a number of substrates by thermal MOCVD.

#### *2.1.1. Perovskite-Type Substrates: $NdGaO_3$ and $SrTiO_3$*

Neodymium gallate has a good crystallographic match with $LaAlO_3$ (mismatch 2.45 %). At 1000 °C we obtained high-quality epitaxial (001)$LaAlO_3$/(001)$NdGaO_3$ films as indicated by XRD $\theta$–$2\theta$ and $\phi$ scans (Fig. 1A,B), and the

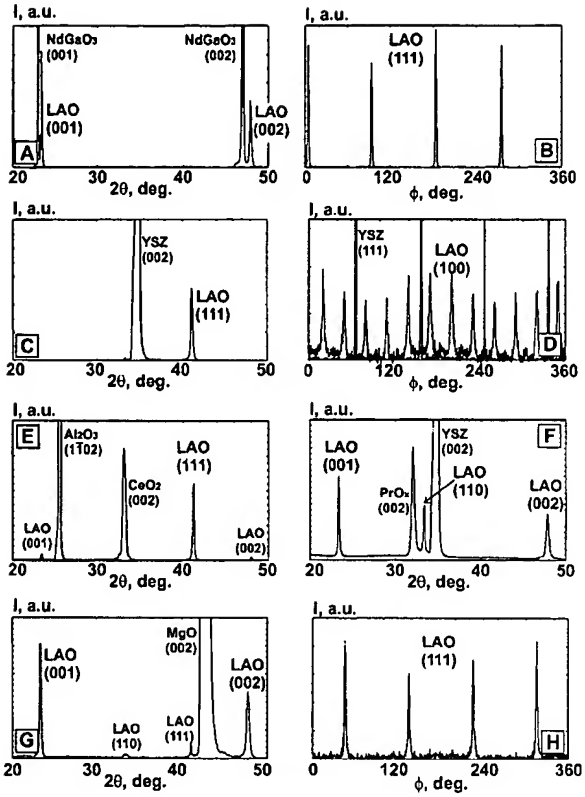


Fig. 1. XRD data for $LaAlO_3$ films deposited at 1000 °C: A) $\theta$–$2\theta$ scan for (001)$LaAlO_3$/(001)$NdGaO_3$. B) $\phi$ scan for (001)$LaAlO_3$/(001)$NdGaO_3$ confirming in-plane alignment. C) $\theta$–$2\theta$ scan for (111)$LaAlO_3$/(001)YSZ. D) $\phi$ scan for (111)$LaAlO_3$/(001)YSZ, revealing two type in-plane alignment. E) $\theta$–$2\theta$ scan for (111) + (001)$LaAlO_3$/(001)$CeO_2$/(1$\bar{1}$02)$Al_2O_3$. F) $\theta$–$2\theta$ scan for (001) + (110)$LaAlO_3$/(001)$PrO_x$/(001)YSZ. G) $\theta$–$2\theta$ scan for (001)$LaAlO_3$/(001)MgO. H) $\phi$ scan for (001)$LaAlO_3$/(001)MgO, confirming in-plane alignment.

$LaAlO_3$ (002) rocking curve full width at half maximum (FWHM) value of 0.54°. At 900 °C, crystalline $LaAlO_3$ films were obtained on $NdGaO_3$; moreover, despite low XRD peak intensity, the films were highly (00*l*) textured. $LaAlO_3$ films grown at 900 °C on the other substrates were amorphous.

We also deposited $LaAlO_3$ films on another coherent perovskite substrate (110)$SrTiO_3$ at 1000 °C. According to the XRD data, (110)$LaAlO_3$/(110)$SrTiO_3$ films were obtained.

It is not surprising that the best results in the growth of perovskite $LaAlO_3$ films can be obtained on coherent perovskite substrates, because there is only a slight difference in lattice constants, which does not favor epitaxy, whereas, in the case of other substrates, the difference in the structure of the matching lattices is also very important.

#### *2.1.2. Fluorite-Type Substrate: YSZ and Buffer Layers $PrO_x$ and $CeO_2$*

Films obtained on (001)YSZ at 950 °C were polycrystalline, at 1000 °C (111)-oriented $LaAlO_3$ films were grown. As is seen from the XRD $\phi$ scan (Fig. 1D), there are two

equivalent in-plane orientations for (111)$LaAlO_3$ growth on (001)YSZ. The following epitaxial relations were established: (111)$LaAlO_3$//(001)YSZ, $\langle\bar{1}10\rangle LaAlO_3$//$\langle100\rangle$YSZ; and (111)$LaAlO_3$//(001)YSZ, $\langle\bar{1}10\rangle LaAlO_3$//$\langle010\rangle$YSZ.

Matching of oxygen positions in the (001)substrate plane and the (111)$LaAlO_3$ plane is shown schematically in Figure 2. Six {100}-type planes of pseudo-cubic lattice give rise

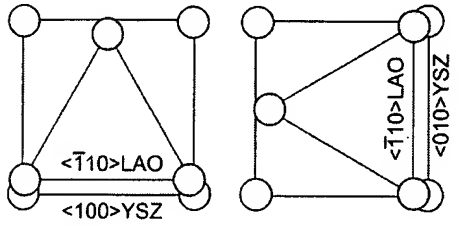


Fig. 2. Model of oxygen cell lattice matching for (111)$LaAlO_3$ and (001)YSZ planes. Epitaxial relations are as follows: (111)$LaAlO_3$// (001)YSZ, $\langle\bar{1}10\rangle LaAlO_3$//$\langle100\rangle$YSZ; (111)$LaAlO_3$//(001)YSZ, $\langle\bar{1}10\rangle LaAlO_3$// $\langle010\rangle$YSZ.

to six symmetrical peaks in the $\phi$ scan with maxima at $n \times 60°$. Due to the presence of two epitaxial in-plane variants, which can be made coincident by 90° rotation around the [001]YSZ direction, twelve peaks are present in the resulting $\phi$ scan (with maxima at $n \times 60°$ and $n \times 60 + 90°$). The same growth behavior had previously been reported for another perovskite-on-fluorite heteroepitaxial pair (111)$BaTiO_3$/(001)YSZ.[12] It is interesting to note that perovskites with lattice parameter values between those for $LaAlO_3$ ($a$ = 3.79 Å) and $BaTiO_3$ ($a$ = 3.94 Å, $c$ = 4.04 Å) such as $CaRuO_3$ and $(La_{1-x}Pr_x)_{0.3}Ca_{0.7}MnO_3$,[13] exhibit different preferential axial alignment (110)perovskite/(001)YSZ.

Two types of texture were found in $LaAlO_3$ films grown on fluorite-type buffer layer $CeO_2/(1\bar{1}02)Al_2O_3$. only (00$l$) and ($hhh$) reflections were present on $\theta$–$2\theta$ scans (Fig. 1E), the latter texture being stronger. Interestingly, (00$l$) and (110) two type textured $LaAlO_3$ films were obtained on another fluorite-type buffer layer $PrO_x$/(001)YSZ (Fig. 1F). A similar result had previously been reported for $BaTiO_3$ films: (111)$BaTiO_3$/(001)YSZ, (111) + (00$l$)$BaTiO_3$/ (001)$CeO_2/(1\bar{1}02)Al_2O_3$, and (00$l$)$BaTiO_3$/(001)$PrO_x$/ (001)YSZ oriented films had grown.[12]

### 2.1.3. NaCl Structure Type Substrate: MgO

We succeeded in depositing (001)$LaAlO_3$/(001)MgO films at temperatures not lower than 1000 °C, as illustrated by XRD $\theta$–$2\theta$ and $\phi$ scans (Fig. 1G,H). It should be noted that (001)-oriented $LaAlO_3$ films are very promising as buffer layers for the deposition of various perovskite films on MgO substrates. Such a buffer layer may change the preferred orientation of perovskite growth on MgO from polycrystalline or slightly textured to epitaxial.

### 2.1.4. Corundum Structure Type Substrate: $\alpha$-$Al_2O_3$

In the deposition temperature range 950–1000 °C, we obtained polycrystalline $LaAlO_3$ films without any pronounced texture, which we assume is due to the large structural mismatch between these materials.

## 2.2. $LaAlO_3$ Films Deposited Using VSA MOCVD

### 2.2.1. MOCVD of $LaAlO_3$ Films in the Presence of $BiPh_3$: Comparison with Bi-free Depositions

We estimated the partial pressure of $Bi_2O_3$ in the reactor, assuming that the whole amount of $BiPh_3$ precursor reacted in the vicinity of the substrate to produce $Bi_2O_3$. By this estimation we got the highest possible value of $Bi_2O_3$ partial pressure. $BiPh_3$ transport to the reactor was achieved with no condensation of bismuth oxide on the substrate, i.e., the $Bi_2O_3$ partial pressure was lower than the $Bi_2O_3$ equilibrium pressure under the deposition conditions. In fact, the gaseous phase over condensed $Bi_2O_3$ contains a number of species: $Bi_2O_3$, Bi, BiO, $Bi_4O_6$, etc.[14] We used data from Kazenas and Chizhikov[14] for the total equilibrium $Bi_2O_3$ pressure, $P_{satur}$, and estimated the relative partial pressure, $P_r = P(Bi_2O_3)/P_{satur}$, for each deposition run.

As expected, energy dispersive X-ray (EDX) and Rutherford back-scattering (RBS) analyses detected no Bi in $LaAlO_3$ films deposited in the presence of $BiPh_3$ (Fig. 3). This correlated with the prediction of thermodynamics because the $Bi_2O_3$ partial pressure in the reactor was kept below the $Bi_2O_3$ equilibrium pressure. The next important result we got was a significant increase of the film deposition rate in the presence of $BiPh_3$, compared with that for the films deposited without $BiPh_3$ with the same supersaturation in the reactor. A deposition rate increase of up to five times (from 0.5 $\mu m\,h^{-1}$ for depositions without $BiPh_3$ to 2–2.5 $\mu m\,h^{-1}$ for depositions in the presence of $BiPh_3$) was observed. This approach has great potential in that it achieves high deposition rates with minimal consumption of precursors.

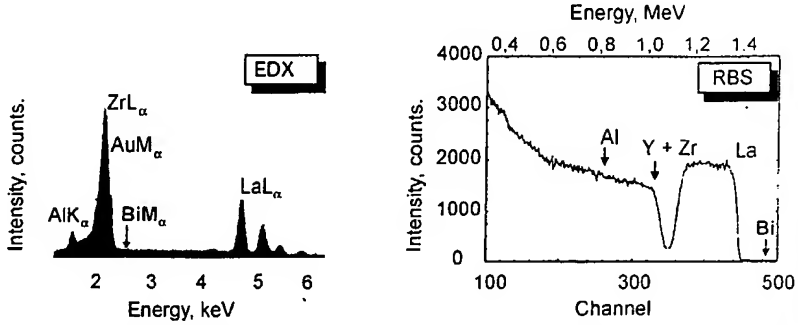


Fig. 3. EDX and RBS spectra demonstrate the absence of bismuth in the $LaAlO_3$/(001)YSZ films deposited in the presence of $BiPh_3$.

  0948-1907/00/0306-0135 $ 17.50+.50/0 

More importantly, crystalline quality and surface morphology were found to improve remarkably for $LaAlO_3$ films deposited in the presence of $BiPh_3$. Thus, $LaAlO_3$ films obtained at relatively low temperatures (800–900 °C) without $BiPh_3$ were amorphous, whereas deposition in the presence of $BiPh_3$ resulted in crystalline films. According to XRD $\theta$–$2\theta$ and $\phi$ scans, epitaxial $LaAlO_3$ films at 950–1000 °C were obtained both with and without the addition of $BiPh_3$ to the starting solution. The addition of $BiPh_3$ led to a pronounced increase in the epitaxial quality of the films as indicated by FWHM values of XRD rocking curves, high-resolution electron microscopy (HREM), and atomic force microscopy (AFM) data. Comparison of the results for the $LaAlO_3$ films, deposited at various $BiPh_3$ feeding rates, demonstrates progressive decrease of FWHM values of (002) rocking curves with the increase of $P_r$ value: 0.65°, 0.52°, and 0.42° at $P_r$ = 0, 0.1, and 0.2, respectively (Fig. 4). HREM investigation showed higher mosaicism and less perfect interface structure in $LaAlO_3$/$NdGaO_3$ films grown without $BiPh_3$ (Fig. 5). AFM also revealed a remarkable difference in surface morphology, indicating higher surface diffusion of the film components during growth in the presence of Bi-containing vapor. The films deposited in the presence of $BiPh_3$ had smoother surfaces (they were characterized by lower values of root-mean-square roughness, see Fig. 6).

It is worth reiterating that all these results were obtained for films deposited in the presence of $BiPh_3$ at a growth rate four to five times higher than that for those deposited without $BiPh_3$. This fact emphasizes how strongly the diffusion mobility in the growing film can be accelerated by the approach proposed.

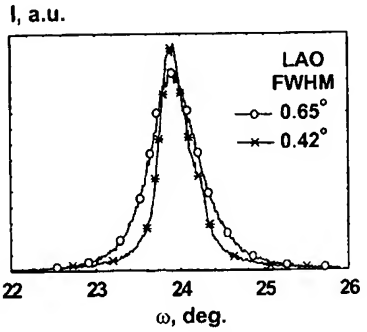


Fig. 4. XRD rocking curves for (002) reflections of (001)$LaAlO_3$/(001)$NdGaO_3$ epitaxial films deposited at 950 °C with (–x–), and without (–O–) the addition of $BiPh_3$. The FWHM value of the rocking curve of the film deposited in the presence of $Bi_2O_3$ is notably smaller.

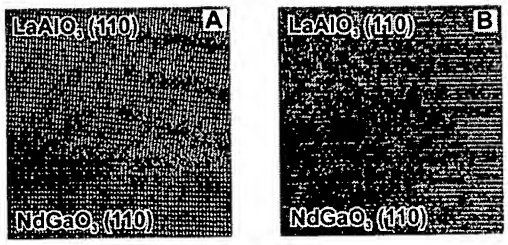


Fig. 5. HREM images of the interfaces of (001)$LaAlO_3$/(001)$NdGaO_3$ epitaxial films deposited at 950 °C: A) without $Bi_2O_3$ and B) in the presence of $Bi_2O_3$.

### 2.2.2. *Proposed Mechanism of Diffusion Mobility Enhancement: VSA MOCVD*

The mechanism of diffusion mobility enhancement in MOCVD (in the presence of $Bi_2O_3$ formed from $BiPh_3$)

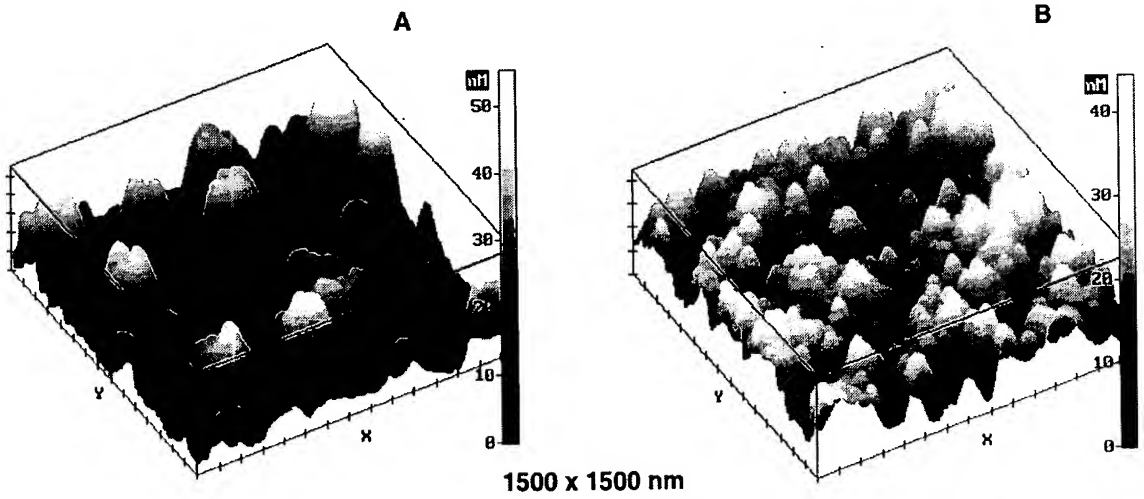


Fig. 6. AFM data on the surface morphology of (001)$LaAlO_3$/(001)$NdGaO_3$ epitaxial films deposited at 950 °C: A) without $Bi_2O_3$, root-mean-square roughness $S_\alpha$ = 8.8 nm, and B) in the presence of $Bi_2O_3$ ($P_r$ = 0.2), $S_\alpha$ = 5.9 nm.



0948-1907/00/0306-0136 $ 17.50+.50/0

Chemical Vapor Deposition

should be clarified. The proposed model of this process is shown schematically in Figure 7.

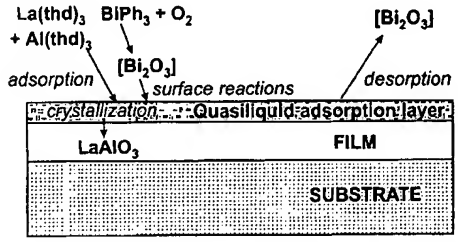


Fig. 7. Proposed mechanism of VSA MOCVD. The model involves adsorption of the precursors, surface reaction producing oxides, formation of a quasiliquid adsorption layer with $Bi_2O_3$, which enhances the crystallization, and desorption of volatile $Bi_2O_3$.

We assume that $BiPh_3$ molecules from the bulk gas flow diffuse through the boundary layer and adsorb on the substrate surface; hence surface reaction takes place, producing bismuth oxide. Other MOCVD reaction products are being formed from the other precursors at the same time (in our case $LaAlO_3$) but, importantly, these condensed particles are not yet crystalline. Bismuth oxide has a low melting temperature (820 °C) and is known to form low melting point eutectics with many oxides. Liquid $Bi_2O_3$ is widely used as a solvent for many oxides in crystal growth by the flux technique.[14] At the deposition temperatures employed in this study, there should be a certain amount of liquid phase on the substrate: $LaAlO_3$ solution in $Bi_2O_3$. Then, crystallization of $LaAlO_3$ occurs from the melt. The mobility of the film components is, naturally, much higher in the liquid phase than on the solid substrate surface. There are numerous examples of crystal growth acceleration owing to the presence of a liquid, the vapor–liquid–solid (VLS) technique[15] being one of the most prominent ones. Consequently, we expected the crystal quality of the resulting film to be essentially higher in the case of crystallization assisted by liquid, and this was clearly confirmed by our experimental results. Moreover, the sticking coefficient for adsorption of the precursors on the substrate covered with liquid should be much higher than that for adsorption on the solid substrate surface at the same precursor concentration in the gas phase. This is the most probable explanation of the observed increase of the deposition rate in the presence of $BiPh_3$, as in the case of VLS (whisker growth).

$Bi_2O_3$ has a sufficiently high saturation vapor pressure to evaporate continuously from the substrate. Because the $Bi_2O_3$ partial pressure in the reactor was kept lower than the $Bi_2O_3$ equilibrium pressure by feeding in appropriate amounts of $BiPh_3$ precursor, no condensation of bulk liquid $Bi_2O_3$ occurs during the deposition. There is a dynamic steady state on the substrate: liquid $Bi_2O_3$ forms and evaporates continuously. Very similar behavior has been described in the literature: under appropriate conditions, self-limiting incorporation of Bi during deposition of Bi-containing ferroelectric $Bi_4Ti_3O_{12}$,[16] and superconductor $Bi_2Sr_2CuO_y$,[17] films occurred. That is, no extra stoichiometric Bi deposited (despite a large extra flux of Bi) because the partial pressure of corresponding Bi-containing particles in vapor was kept higher than their equilibrium pressure over the film compounds, and lower than that over pure Bi or $Bi_2O_3$.

Thus, we believe it is more correct to speak about a more or less thick quasiliquid $Bi_2O_3$ surface adsorption layer, than about a bulk amount of liquid. This adsorption layer can "dissolve" $LaAlO_3$ to some extent, making its diffusion mobility much higher, which improves the crystal quality of the film. Additionally, continuous evaporation of $Bi_2O_3$ from the substrate provides supersaturation of the adsorption layer with the dissolved film components necessary for their crystallization.

The approach that we propose seems to resemble surfactant mediated layer-by-layer growth in the molecular beam epitaxy (MBE) of semiconductors and metals.[18,19] The term "surfactant" is used here in a rather broad sense to denote a surface impurity substance that is added in amounts not exceeding one monolayer, and promotes layer-by-layer growth under conditions at which island homo- or heteroepitaxial growth usually occurs. A good surfactant must float on the surface of the growing film without being incorporated, and must not form a separate phase. These conditions are met when the effective bond strengths satisfy the inequalities $V_{A-A} > V_{A-S} >> V_{S-S}$, where A and S are adatoms of the growing substance and the surfactant atoms, respectively.[20] Although the mechanisms of surfactant-mediated epitaxy and the approach to MOCVD proposed by us can be essentially different, we believe the criteria of applicability for volatile low melting point oxides should be almost the same as those for surfactants; therefore, we decided to use the term "surfactant" (in an analogous, broad sense) to denote volatile low melting point oxides in our approach.

We proposed the term volatile surfactant-assisted MOCVD (VSA MOCVD) for this version. The crystal growth mechanism in VSA MOCVD has obviously many common features with VLS and flux techniques. Consequently, the main approaches and considerations developed for these techniques[15,16] may be useful also in VSA MOCVD. On the other hand, there are some clear distinctions. First, in VSA MOCVD, there is no bulk liquid phase, which makes it possible for $Bi_2O_3$ to cover the entire substrate surface uniformly without combining in separate droplets, as in VLS. Second, liquid surfactant $Bi_2O_3$ is produced on the substrate in situ, not the case in the aforementioned techniques. It enhances the crystallization, making the film components more mobile, and leaves the substrate completely by the end of the process.

There is a limitation to the proposed approach that should be mentioned here: the volatile surfactant chosen should not form stable compounds, or an extended solid solution range, with the components of the film to be obtained (this is expressed by $V_{A-A} > V_{A-S}$). In this work,

  0948-1907/00/0306-0137 $ 17.50+.50/0 

from a number of volatile low melting point oxides, we chose bismuth oxide; however, there are possible surfactants that might prove interesting, such as PbO, $MoO_3$, $Tl_2O$, etc. It is also interesting to try combinations of oxides (e.g., PbO + $Bi_2O_3$), like the complex solvents in the flux technique.

## 3. Conclusions

We have developed volatile surfactant-assisted MOCVD, a new approach to the CVD of oxide films with kinetically hindered diffusion, first proposed in our previous work.[12] The approach involves film deposition in the presence of a volatile low melting point oxide, in our case $Bi_2O_3$ was selected. The process was applied to the deposition of $LaAlO_3$ films, and a model of the process was proposed.

We succeeded in the deposition of epitaxial and textured $LaAlO_3$ films on various substrate materials, both by thermal and VSA versions of MOCVD. The following axial orientations were found in the films: (001)$LaAlO_3$//(001)$NdGaO_3$; (001)$LaAlO_3$//(001)MgO; polycrystalline $LaAlO_3/(1\bar{1}02)Al_2O_3$; (111)$LaAlO_3$//(001)YSZ; (111) + (001)$LaAlO_3$//(001)$CeO_2/(1\bar{1}02)Al_2O_3$; (001) + (110)$LaAlO_3$//(001)$PrO_x$/(001)YSZ.

The crystalline quality and surface morphology were found to improve remarkably for the films deposited in the presence of $Bi_2O_3$, compared with those grown without $Bi_2O_3$. According to EDX and RBS analysis, $LaAlO_3$ films obtained in the presence of $Bi_2O_3$ did not contain Bi. Significant increase (up to five times) of the film deposition rate was observed for $LaAlO_3$ films deposited in the presence of $Bi_2O_3$, compared with that for the films grown without $Bi_2O_3$.

The experimental results obtained thus far are in good agreement with the proposed VSA MOCVD mechanism although they cannot be considered to be final confirmation since further study of the mechanism, using direct observation, is necessary. On the other hand, we believe that VSA MOCVD shows potential as a method of obtaining various oxide films. Judging by the results obtained, VSA MOCVD is a promising method of depositing high-quality epitaxial films, crystalline films of the phases with kinetically hindered diffusion, and growing films and coatings at high deposition rates.

## 4. Experimental

Film depositions were carried out with a single aerosol source MOCVD setup, described in detail elsewhere [21], which has been used to deposit various oxide films such as $YBa_2Cu_3O_{7-y}$, $Bi_2Sr_2CaCu_2O_x$ [21], $(La_{1-x}Pr_x)_{0.7}Ca_{0.3}MnO_3$ [13], $La_{1-x}Sr_xCoO_3$ [22], and $BaTiO_3$ [12]. Briefly, a solution of the precursors is nebulized ultrasonically and the aerosol thus produced flows with the Ar carrier gas into a heated tube where evaporation of the solvent and precursors takes place. The vapor is transported through heated lines by Ar flow into the vertical cold wall reactor. A solution of $La(thd)_3$, $Al(thd)_3$, and, in some experiments, $BiPh_3$ precursors in diglyme was used. In order to avoid ligand exchange with $BiPh_3$, 3 vol.-% Hthd was added in the starting solution [12].

The films were characterized by XRD $\theta$–$2\theta$ and $\phi$ scans, and rocking curve and pole figure measurements performed with a Siemens D5000 four circle diffractometer with a secondary graphite monochromator (Cu K$\alpha$ radiation). Film microstructure and composition were studied using a CAMSCAN scanning electron microscope equipped with an EDAX system for quantitative analysis. RBS spectroscopy (Van der Graaf accelerator, 1.5 MeV $He^+$ ions) was used to analyze traces of the surfactant in the films, film thickness, and composition. Transmission electron microscopy was performed with a Philips CM30ST electron microscope operating at 300 kV and equipped with a field emission gun and side-entry ±25° tilt specimen holder. The film thickness was also measured using an alpha-step 200 profilometer (Tencor Instruments) and estimated from EDX spectra. The surface morphology was studied using AFM (P4-SPM-MDT, Nanotechnology MDT Inc., Russia).

Received: March 9, 1999
Final version: November 29, 1999

[1] H. Suhr, *Surf. Coat. Technol.* **1991**, *49*, 233.
[2] P. C. Chou, Q. Zhong, Q. L. Li, K. Abazajian, A. Ignatiev, C. Y. Wang, E. E. Deal, J. G. Chen, *Physica C* **1995**, *254*, 93.
[3] H. Ohnishi, K. Hanaoka, Y. Goto, H. Harima, K. Tachibana, *Physica C* **1991**, *190*, 134.
[4] H. O. Pierson, *Handbook of Chemical Vapor Deposition: Principles, Technology and Applications*, Noyes, Park Ridge, NJ **1992**.
[5] I. E. Graboy, A. R. Kaul, N. V. Markov, V. V. Maleev, I. E. Korsakov, O. Yu. Gorbenko, A. A. Molodyk, *Electrochem. Soc. Proc.* **1997**, *97-25*, 925.
[6] C. M. Carlson, J. C. Price, P. A. Parilla, D. S. Ginley, D. Niles, R. D. Blaugher, A. Goyal, M. Paranthaman, D. M. Kroeger, D. K. Christen, *Physica C* **1998**, *304*, 82.
[7] L. P. Lee, K. Char, M. S. Colclough, G. Zaharchuk, *Appl. Phys. Lett.* **1991**, *59*, 3051.
[8] A. E. Lee, C. E. Platt, J. F. Burch, R. W. Simon, J. P. Goral, M. M. Al-Jassim, *Appl. Phys. Lett.* **1990**, *57*, 2019.
[9] S. S. Shoup, M. Paranthaman, D. B. Beach, E. D. Specht, R. K. Williams, *J. Mater. Res.* **1997**, *12*, 1017.
[10] G. Malandrino, I. L. Fragalà, *Electrochem. Soc. Proc.* **1997**, *97-25*, 844.
[11] G. Malandrino, I. L. Fragalà, P. Scardi, *Chem. Mater.* **1998**, *10*, 3765.
[12] O. Yu. Gorbenko, A. R. Kaul, G. Wahl, *Chem. Vap. Deposition* **1997**, *3*, 193.
[13] O. Yu. Gorbenko, A. R. Kaul, A. A. Molodyk, V. N. Fuflyigin, M. A. Novozhilov, A. A. Bosak, U. Krause, G. Wahl, *J. Alloys Compd.* **1997**, *251*, 337.
[14] E. K. Kazenas, D. M. Chizhikov, *Vapor Pressure and Vapor Composition of Oxides of Chemical Elements*, Nauka, Moscow, **1976** (in Russian).
[15] L. M. Viting, *High Temperature Melt Solutions*, Moscow State University Edition, Moscow **1991** (in Russian).
[16] R. S. Wagner, W. C. Ellis, *Appl. Phys. Lett.* **1964**, *4*, 89.
[17] C. D. Thies, J. Yeh, D. G. Schlom, M. E. Hawley, G. W. Brown, J. C. Jiang, X. Q. Pan, *Appl. Phys. Lett.* **1998**, *72*, 2817.
[18] S. Migita, Y. Kasai, H. Ota, S. Sakai, *Appl. Phys Lett.* **1997**, *71*, 3712.
[19] M. Copel, M. C. Reuter, E. Kaxiras, R. M. Tromp, *Phys. Rev. Lett.* **1989**, *63*, 632.
[20] Zh. Zhang, M. G. Lagally, *Phys. Rev. Lett.* **1994**, *72*, 693.
[21] O. Yu. Gorbenko, V. N. Fuflyigin, Yu. Yu. Erokhin, I. E. Graboy, A. R. Kaul, Yu. D. Tretyakov, G. Wahl, L. Klippe, *J. Mater. Chem.* **1994**, *4*, 1585.
[22] O. Yu. Gorbenko, V. A. Amelichev, J. A. Rebane, A. R. Kaul, *Electrochem. Soc. Proc.* **1997**, *97-25*, 1093.

  0948-1907/00/0306-0138 $ 17.50+.50/0 